Journal of Inorganic Biochemistry 208 (2020) 111082

Contents lists available at ScienceDirect

Journal of Inorganic Biochemistry

journal homepage: www.elsevier.com/locate/jinorgbio

New *in vitro* highly cytotoxic platinum and palladium cyanoximates with minimal side effects *in vivo*

Stephanie D. Dannen[a], Lauren Cornelison[b], Paul Durham[b], John E. Morley[c], Kiana Shahverdi[d], Junwei Du[e], Haiying Zhou[d], Leland C. Sudlow[d], Daniel Hunter[f], Matthew D. Wood[f], Mikhail Y. Berezin[d,e,*], Nikolay Gerasimchuk[a,*]

[a] Department of Chemistry, Temple Hall 431, Missouri State University, 901 S. National, Springfield, MO 65897, USA
[b] Department of Biology, Missouri State University, MC/Center for Biomedical & Life Sciences, Springfield, MO 65897, USA
[c] Division of Geriatric Medicine, Saint Louis University, St. Louis, MO 63110, USA
[d] Department of Radiology, Washington University School of Medicine, St. Louis, MO 63110, USA
[e] Institute of Materials Science and Engineering, Washington University in St. Louis, St. Louis, MO 63130, USA
[f] Department of Medicine, Washington University School of Medicine, St. Louis, MO 63110, USA

ARTICLE INFO

Keywords:
Pd/Pt-cyanoximates
Crystal structures
Human cancer cells
in vitro studies
Animal model
in vivo studies

ABSTRACT

Several biologically active bivalent Pd and Pt complexes with two structurally similar cyanoxime ligands abbreviated as H(DECO): 2-oximino-2-cyano-N,N′-diethylacetamide, and H(PyrCO): 2-oximino-2-cyan-N-pyrrolidine acetamide were synthesized and characterized using spectroscopic methods, thermal analysis and X-ray crystallography. Structures revealed planar cis-geometry of studied complexes. Freshly obtained $Pt(DECO)_2$, $Pd(DECO)_2$, $Pt(PyrCO)_2$ and $Pd(PyrCO)_2$ complexes were used in for *in vitro* cytotoxicity assays using two different etiology human cancer cell lines HeLa and WiDr cells. Investigated compounds showed cytotoxicity levels at or above cisplatin. $Pt(DECO)_2$ was also tested *in vivo* in healthy C57BL/6 mice. The complex was administered at three different dosage (0, 7.5, 15 mg/kg, i.p. once/week), over a total period of 8 weeks. No changes were observed in the animal weight in the treated mice compared to the control dextrose-treated group. The levels of erythrocytes, leukocytes, and hemoglobin were within the normal level suggesting low myelotoxicity. Negligible cardiotoxicity was observed from the histological evaluation of the hearts from the treated animals. Results from the tail nerve conduction velocity (NCV) and nerve histomorphometry suggested no impact of $Pt(DECO)_2$ on peripheral nerves. The complex, however, induced certain hepatotoxicity and lead to the elevation of IL-6, a pro-inflammatory cytokine. Overall, Pt(DECO)2 showed minimal *in vivo* toxicity, thus presenting a promising candidate for future testing in animal models of cancer.

1. Introduction

Platinum-based compounds, such as cisplatin, carboplatin, and oxaliplatin are among the most commonly prescribed chemotherapeutic agents [1]. One of the common problems with many chemotherapy drugs, including platinum complexes, is their strong side effects that weaken the immune system [2], trigger anemia [3], damage cardiovasculature, induce muscle loss [4], and cause neurological deficits and pain [5]. The responses are usually drug-dependent. For example, cisplatin has been specifically connected to neurotoxicity, adverse gastrointestinal effects, and renal function impairment [6]. Carboplatin-containing chemotherapy has been more associated with myelosuppression, and high incidence of severe neutropenia and anemia [6]. Finding suitable alternatives to the existing platinum-based therapies with high anticancer efficiency and low side effects is an ongoing clinical and research goal.

Organometallic complexes with cyanoxime ligands might present a viable option. Cyanoximes are low molecular weight ampolydentate organic ligands of general formula NC-(C=N-OH)–R which have received attention in recent years due to their pronounced biological activity and interesting properties [7]. Previous publications have shown that pairing these ligands with platinum(II) and palladium(II) has resulted in the formation of complexes with substantial *in vitro* cytotoxic activity against HeLa (cervical adenocarcinoma) and WiDr (colon adenocarcinoma) cell lines [8,9]. Of the 42 cyanoximes known today [10], there are still a large number of complexes that have not yet been evaluated in biological settings.

* Corresponding authors.
E-mail addresses: berezinm@wustl.edu (M.Y. Berezin), NNGerasimchuk@MissouriState.edu (N. Gerasimchuk).

https://doi.org/10.1016/j.jinorgbio.2020.111082
Received 16 February 2020; Received in revised form 28 March 2020; Accepted 28 March 2020
Available online 06 May 2020

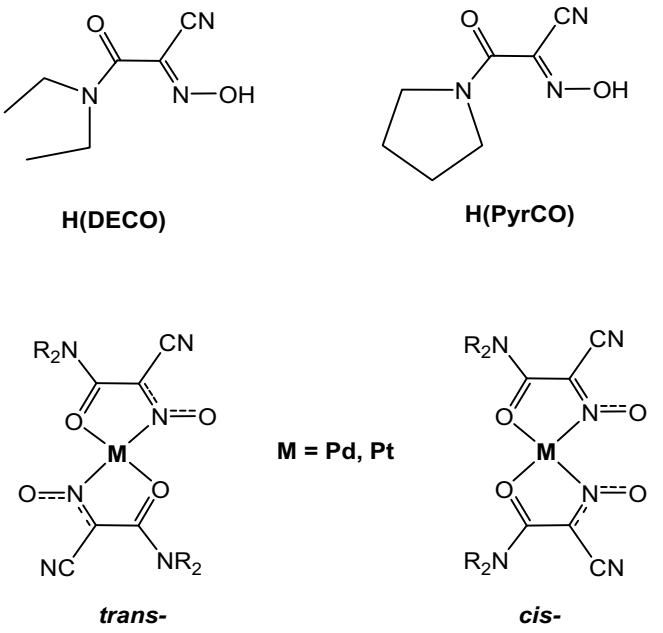

Fig. 1. Structures of cyanoximes used in this study. Each ligand molecule can form metallocomplexes of cis- and trans- geometries. DECO: 2-oximino-2-cyano-N,N′-diethylacetamide, PyrCO: 2-oximino-2-cyan-N-pyrrolidine acetamide. (For interpretation of the references to colour in this figure legend, the reader is referred to the web version of this article.)

Given the potential of the cyanoximate complexes in cancer treatment, testing the *in vitro* activity and *in vivo* toxicity of these molecules is instrumental in discovering a new class of novel chemotherapy drugs with potentially low side effects.

Herein, we investigated several existing and new members of the Pt and Pd cyanoxime complexes (Fig. 1) *in vitro* using common HeLa and WiDr cancer cell lines. To assess the toxic side effects in live animals, we administered multiple doses of Pt(II) 2-oximino-2-cyano-N,N′-diethylacetamide abbreviated as $Pt(DECO)_2$ to healthy C57BL/6 mice at two different levels (7.5 mg/kg and 15 mg/kg) once per week over an 8 week period. The highest dose (15 mg/kg) corresponded to a typical maximal tolerable single dose of cisplatin that can be administered to normal mice. Control animals were injected with the equivalent volume of a dextrose solution with no platinum complex added. The established markers of side effects such as weight change, complete blood count, cytokine level, and nerve conduction velocity were recorded in live animals. The study was completed by histological evaluation of the sciatic nerve and the heart to estimate the level of peripheral neuropathy and cardiotoxicity.

2. Experimental section

2.1. Synthesis and characterization of complexes

2.1.1. General considerations

The common chemicals and solvents were all reagent grade (Aldrich, WI) and used without further purification. Sources of Pd and Pt were available as tetrachloro-salts of $K_2[MCl_4]$ (M = Pd, Pt) composition from Pressure Chemical Company (Pittsburgh, PA). The TLC for ligands' identification were carried out on silica-coated glass plates (Merck) with a 256 nm fluorescent indicator. Elemental analyses on C, H, N content were performed at Atlantic Microlab (Norcross, GA). Melting points for organic compounds were measured on a Digimelt™ apparatus without correction.

2.1.2. Synthesis of H(DECO) and H(PyrCO) ligands

Both these cyanoximes were prepared at room temperature under N_2 atmosphere as a result of reaction within several minutes between neat cyanoacetic ester and $HN(C_2H_5)_2$ (for H(DECO)) and pyrrolidine (for H(PyrCO)) (Scheme 1). Resulting white waxy solids were filtered off, washed with cold methanol, then with anhydrous benzene and then dried in vacuum desiccator over H_2SO_4(c). The next step was the nitrosation reaction that was carried out by slow bubbling of gaseous methylnitrite CH_3-ONO within ~15 min through *n*-propanol solutions of appropriate substituted acetonitrile in the presence of freshly prepared *in situ* sodium propoxide [11]. The reaction mixture was concentrated on a rotary evaporator to give yellow sludge that was solidified under an oil pump vacuum. To the yellow solid ~50 mL of distilled water were added at once with the formation of a bright-yellow solution. Diluted HCl(aq) solution (1:5) was then added dropwise to bring pH of the mixture from 12 to ~3. Excess of solid NaCl was added to that solution to form brine, and extraction of desired cyanoxime was performed using three portions of 20, 30 and 50 mL of ether. Slightly yellow colored organic layers were combined and dried over anhydrous Na_2SO_4 overnight at +4 °C in a refrigerator. Ether was removed on a rotary evaporator to give off-white solids of H(DECO) and H(PyrCO) oximes. The solids were then re-dissolved in dry ether, mixed with a spatula of Norite© and then filtered through Celite© to give transparent solutions. Solvent removal provided colorless crystalline compounds.

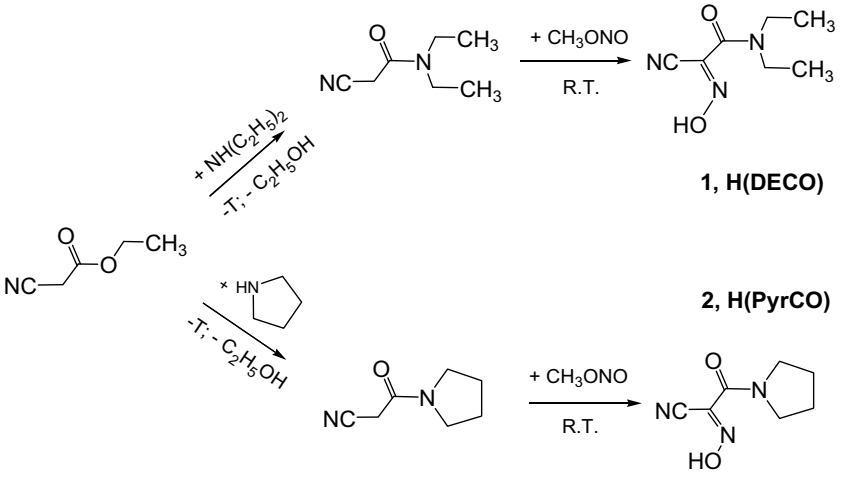

Scheme 1. Synthetic routes to H(DECO) and H(PyrCO) amide-based cyanoximes.

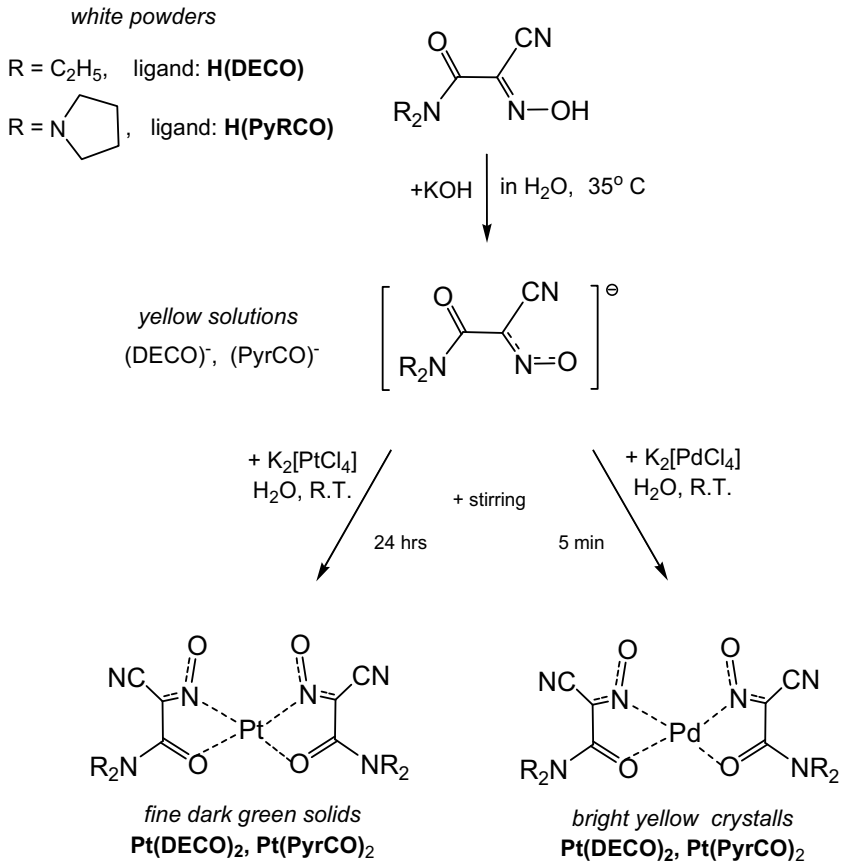

Scheme 2. Synthesis of Pt and Pd -based cyanoximines.

2.1.3. Synthesis of metal complexes

The general procedure for other complexes presented in Scheme 2.

2.1.3.1. Pd(DECO)$_2$. H(DECO) is not soluble in water, but after deprotonation with base it becomes soluble which enables reactions with transition-metal salts. Thus, the stoichiometric amount of a 1.01 M KOH solution (1.93 mL) was added to the H(DECO) (1) sludge in water that immediately dissolved with the formation of a bright yellow solution. Another solution of 0.318 g (0.98 mM) of $K_2[PdCl_4]$ in 5 mL of water was added dropwise into the yellow $DECO^-$ solution under intense stirring. A thick yellow precipitate formed instantaneously, and after ~5 min of stirring, it was filtered, washed three times with water, and then dried in a desiccator charged with concentrated H_2SO_4. Elemental analysis: found (calcd) for $PdC_{14}H_{20}N_6O_4$: N, 18.24 (18.24); C, 37.05 (37.05); H, 4.50 (4.50). IR (KBr pellet, cm^{-1}): 2983 [ν^{as}(CH)], 2940 [ν^{s}(CH)], 2211 [ν(C≡N)], 1631 [ν(CO, amide I)], 1440 [ν(CNO), oxime], 1579 [ν(CO, amide II)], 1200 [ν(CNO)]. The complex is soluble in CH_3CN, DMF, DMSO, pyridine, and its homologues, but not well soluble in acetone and alcohols.

2.1.3.2. Pt(DECO)$_2$. The Pt(DECO)$_2$ was obtained in a similar fashion that was reported early [12]. Elemental analysis: Found (calcd) for $PtC_{14}H_{20}N_6O_4$: N, 18.24 (18.24); C, 37.05 (37.05); H, 4.50 (4.50). There were three polymorphs obtained from Pt(II) – DECO system: yellow, red and dark-green (Electronic Supporting Information section, ESI: 1).

2.1.3.3. Pt(PyrCO)$_2$. For the synthesis of Pt(PyrCO)$_2$, 0.217 g (1.28 mM) of H(PyrCO) (2) in 8 mL of water was treated with 1.28 mL of 1.01 M KOH, forming a yellow solution of deprotonated cyanoxime $PyrCO^-$, to which 0.268 g (0.65 mM) of K_2PtCl_4 in 5 mL was added. When all components were mixed, the formation of the Pt (PyrCO)$_2$ complex was observed after an extended period of time. After ~24 h, a very fine dark-green precipitate was filtered (see ESI 2), washed three times with water, and then dried in a vacuum desiccator under concentrated H_2SO_4. Elemental analysis: found (calcd) for green-form $PtC_{14}H_{16}N_6O_4$: N, 15.75 (15.78); C, 31.52 (31.46); H, 4.16 (4.03). IR (KBr pellet, cm^{-1}): 2985 [ν^{as}(CH)], 2943 [ν^{s}(CH)], 2213 [ν(C≡N)], 1709 [ν(CO, carbonyl)], 1622; 1442 [ν(CNO), oxime], 1585 [ν(CO, amide II)], 1227 [ν(CNO)]. The dark-green form is not soluble in water but has some solubility in alcohols, slowly dissolves in DMSO, forming at first a dark-red solution of a dimer $[Pt(PyrCO)_2]_2$. There are three differently colored polymorphs (ESI 2).

2.1.3.4. Pd(PyrCO)$_2$. Pd(PyrCO)$_2$ was obtained in a similar fashion. Elemental analysis: found (calcd) for $PdC_{14}H_{16}N_6O_4$: N, 19.24 (19.16); C, 38.05 (38.33); H, 3.95 (3.68).

2.1.4. IR-spectroscopy

The IR-spectra of all compounds reported herein were recorded in KBr disks at room temperature using the Bruker R70 FT-IR-Raman complex. All spectra were recorded with 64 repetitions at the resolution of 4 cm^{-1}. Data tabulated in the ESI 3.

2.1.5. IR-spectral data

Vibrational spectra of synthesized Pd, Pt complexes contain bands of the ν(C=O) amide and ν(NCO) nitroso groups shifted accordingly to the anions' binding modes. Thus, the amide group frequency is lower than that for uncomplexed cyanoximes, while the band with participation of the C-N-O fragment is shifted to higher wavenumbers as compared to free ligands since it gained *nitroso* character [13].

2.1.6. UV–visible spectra

The electronic spectra of the compounds were recorded at room

temperature using the HP 8354 diode array UV–visible spectrophotometer operating in the range of 200–1100 nm. The absorbance spectra from samples were recorded in solutions and in fine suspensions in mineral oil squeezed between 1 × 4 cm quartz plates. Data of spectroscopic studies are presented in ESI 4–6.

2.1.7. X-ray crystallography

Suitable single crystals of $Pt(DECO)_2$, $Pt(PyrCO)_2$, and $[Pt(PyrCO)_2]_2$ were grown from the DMSO solutions. Large red crystals of the latter dimer appeared overnight. The crystals were collected and placed for handling and selection in thick paratone oil. The yellow crystals of the monomeric complex appeared upon monomerization of the dimeric crystals at ambient conditions from red ones. This fact, in essence, represents a rather unusual crystal-to-crystal conversion of polymorphs spontaneously breaking down from more complex structure to more simple monomeric units. All attempts to grow suitable crystals of the dark-green polymeric $[PtL_2]_n$ complexes (L = $DECO^-$, $PyrCO^-$) were unsuccessful (ESI 7). The crystal structures for the DECO compounds were reported earlier [12]. Structures for the yellow monomeric $Pt(PyrCO)_2$ and its red $[Pt(PyrCO)_2]_2$ dimer are shown below. All crystals selected and suitable for studies were placed on plastic MiTeGen holders attached to the copper-pin on the goniometer head of the Bruker APEX-2 diffractometer, equipped with a SMART CCD area detector. The intensity data were collected at low temperature. Data collection was done in ω scan mode using the Mo tube (K_α radiation; λ = 0.71073 Å) with a highly oriented graphite monochromator. Intensities were integrated from 4 series of 364 exposures, each covering 0.5° steps in ω at 20–60 s of exposition time, with the total data set being a sphere. The space group determination was done with the aid of the XPREP software. The absorption correction was performed by a crystal face indexing procedure with a help of a video microscope (ESI 8) followed by numerical input into the SADABS program that was included in the Bruker AXS software package. All structures were solved by direct methods and refined by least squares on weighted F^2 values for all reflections using the SHELXTL program. In all structures, H-atoms were placed in calculated positions in accordance with the hybridization state of a hosting carbon atom and were refined isotropically. No apparent problems or complications were encountered during the structures' solutions and refinement as evident from a very positive PLATON checkCIF reports. The crystal data for monomeric $Pd(DECO)_2$, $Pt(PyrCO)_2$ and $[Pt(PyrCO)_2]_2$ are presented in ESI 9; Table 3, with selected bond lengths and valence angles presented in ESI 10,11; Tables 4,5. Details of the crystal packing for these three complexes are presented in ESI 12–17. A representative drawing of the crystal structures and packing diagrams was done using the ORTEP and Mercury software packages. Reported structures have been deposited at CCDC at the following numbers: $Pt(PyrCO)_2$ 1,984,335 and $[Pt(PyrCO)_2]_2(DMSO)_2$ 1,984,334, $Pd(DECO)_2$ 1,984,333 with PLATON checkCIF reports presented in at the end of Supporting Information Section in ESI 22.

Structures of all crystallographically characterized here in coordination compounds contain cyanoxime anions in *cis*-orientation to central atoms of Pd or Pt (Figs. 2, 4). This finding is in line with previously determined structures of other cyanoximates of these transition metals [14].

Anions of $DECO^-$ and $PyrCO^-$ are in the *nitroso*-form, and central atoms adopt distorted square-planar *cis*-MN_2O_2 structures of coordination polyhedrons. The nitroso-character of anions is evident from significantly shorter N—O bonds as compared to C—N bonds in the C-N-O fragment (ESI 10, Table 4). In the structure of a red $[Pt(PyrCO)_2]_2{\cdot}(DMSO)_2$ complex monomeric units are arranged *via* short platinophilic interactions into “head-to-tail” dimer (Fig. 3). Red crystals of the dimer left for 20–30 h change to yellow monomer that surprisingly keep the same shape, but lose the solvent molecules. Single crystal specimen suitable for the X-ray analysis was selected from a series of yellow crystals in paratone oil that were red just a day before. The structure of the yellow monomer show no solvent molecules present, DMSO apparently went into the oil.

Indeed, close analysis of the structure of the red dimer evidences importance of the role of DMSO that stabilizes the dimer *via* short

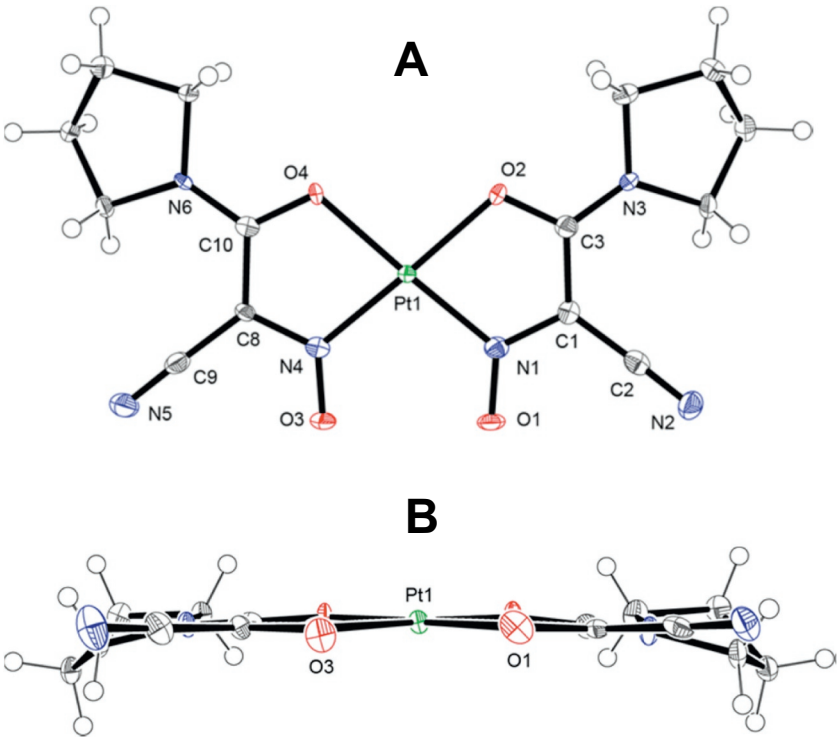

Fig. 2. Crystal structure of yellow monomeric Pt(PyrCO)2: A – top, and B – side views showing ligands' cis-arrangement and planar metal core environment. (For interpretation of the references to colour in this figure legend, the reader is referred to the web version of this article.)

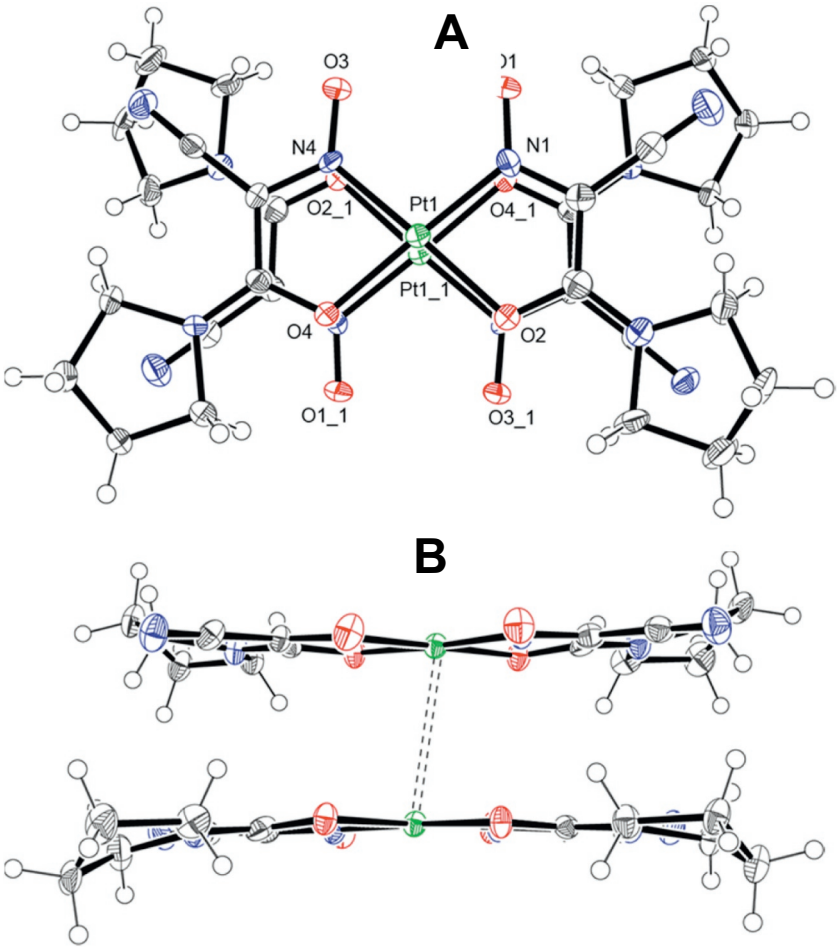

Fig. 3. Crystal structure of red dimeric [Pt(PyrCO)2]2(DMSO)2: A – top view showing dimer's head-to-tail arrangement, and B – side view demonstrating short metallophilic interaction at 3.221 Å. Solvent molecules are omitted for clarity. (For interpretation of the references to colour in this figure legend, the reader is referred to the web version of this article.)

electrostatic C-H—O contacts (ESI 17). This is a similar situation recently observed for the other red dimeric $[Pt(MCO)_2]_2{\cdot}(DMSO)_2$ complex [14].

2.1.8. Thermal Stability Studies

Thermal stability of the obtained metal complexes was assessed using Q-600 TG/DSC analyzer (TA Instruments) under N_2 flow of 100 mL/min at 10°/min heat rate. Heating of samples was carried out to 1000 °C at which the samples' complete decomposition was attained. Results of thermal analyses studies are presented in detail in ESI 18–21.

2.2. In vitro and in vivo evaluation

2.2.1. In vitro cytotoxicity studies

Platinum and palladium cyanoximates $Pt(DECO)_2$, $Pd(DECO)_2$, $Pt(PyrCO)_2$, and $Pd(PyrCO)_2$ were tested *in vitro* for cytotoxicity on cultured HeLa and WiDr cells. The HeLa and WiDr cancer cells (American Type Culture Collection, CCL-2 and CCL-218, respectively) were cultured according to the vendor's recommended procedures. They were maintained at 37 °C with no CO_2 in the incubator in L-15 growth media (Sigma Aldrich, Inc.) containing HEPES buffer, penicillin/streptomycin antibiotic, and 10% fetal bovine serum (Sigma Aldrich). Both cell lines were cultured in 24 well plates at a seeding density of $8{\cdot}10^4$ cells per cm^2. The cells on the plates were grown for 24 h in normal media before any compounds were introduced.

Synthesized Pt and Pd cyanoximates have limited water-solubility. In order to bring them into solution for subsequent mixing with buffered cell culture media DMSO was used in amount not exciding 1% by volume in the final mixture. Platinum and palladium complexes were prepared in 0.1 M concentrations in DMSO, and then further diluted by growth media to 1 mM. Cisplatin was used as a positive control and prepared at the same concentrations as the Pt/Pd complexes. Normal growth media was removed from the wells of each culture plate and replaced with the solutions of interest. Cells were exposed to 1 mM complex in their growth media in two duplicate wells.

2.2.2. Viability assay

The plates of each cell line were incubated for 24 h in the new media. The cells were then assayed using Trypan Blue dye (Sigma) diluted to 0.1% concentration for 2 min at room temperature, washed with PBS, and fixed using 4% paraformaldehyde. This method relies on a breakdown in membrane integrity that is determined by the uptake of

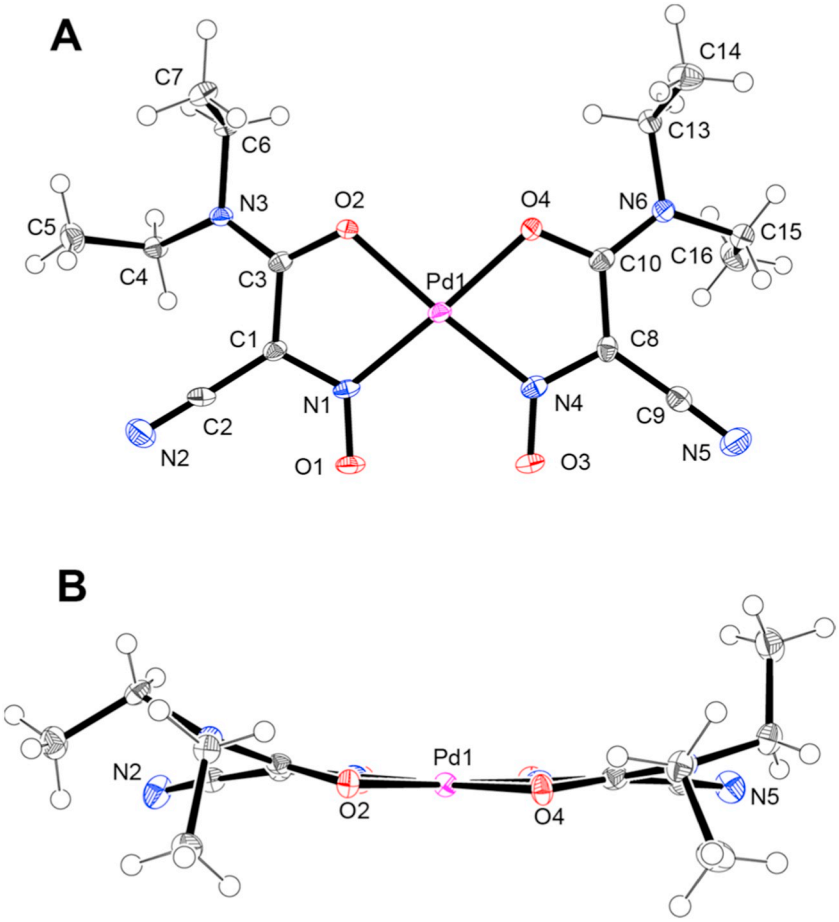

Fig. 4. Crystal structure of yellow monomeric $Pd(DECO)_2$: A – top, and B – side views showing cyanoxime's cis-arrangement in the complex and planar metal center environment. (For interpretation of the references to colour in this figure legend, the reader is referred to the web version of this article.)

a dye, such as Trypan Blue, which is normally membrane impermeable. Cells were viewed using a phase contrast microscope. Digital pictures of the cells were analyzed to evaluate compound toxicity. Two fields of cell views (×40 magnification) from two independent dishes (wells in 24-wells plate) were analyzed for each condition. Random fields of cells were counted, and any blue/dark cells were recorded as nonviable. Thus, cells viability was assessed for each prepared compound and for cisplatin. Cells in pure media and calculated level of DMSO were used as negative controls. The percent of viable cells for each well were averaged and standard deviation was calculated for each plate.

2.2.3. *In vivo studies*

All animal studies were conducted in compliance with the Washington University Institutional Animal Studies Committee and NIH guidelines. C57BL/6 male mice age 8–10 weeks old (Charles River) were randomized to one of three groups: control, 7.5 mg/kg, and 15 mg/kg. Mice were housed in a central animal care facility and provided with food and water *ad libitum*. Animals were kept in standard cages at room temperature and 12 h day/night light cycle.

The mice were injected with freshly prepared $Pt(DECO)_2$ interperiotoneally (ip). Control mice were injected with the similar volume of 5% dextrose solution. Administrations of $Pt(DECO)_2$ were performed weekly, at the same time of the day to eliminate circadian effects.

2.2.4. *Injection preparation*

$Pt(DECO)_2$ powder (~1 mg) was first dissolved in DMSO and then re-dissolved in 5% dextrose prepared by diluting commercial 50% dextrose solution (Phoenix Pharmaceuticals, Inc.). The injection volume per mouse was 200–250 μL depending on the weight of the mouse.

2.2.5. *Nerve histomorphometry*

Sciatic nerves were harvested and stored in 3% glutaraldehyde (Polysciences Inc.). The tissues were post-fixed in 1% osmium tetroxide and serially dehydrated in ethanol and propylene oxide. Stained and dehydrated nerves were then embedded in epoxy (Polysciences), sectioned on an ultramicrotome into 1 μm cross sections, and placed on microscopy slides. Slides were counter-stained with 1% toluidine blue. The slides were then analyzed at 1000× on a Leitz Laborlux S microscope. A semi-automated digital image-analysis system linked to morphometry macros developed for peripheral nerve analysis (Clemex Vision Professional); Clemex Technologies, Longueuil, Québec was utilized to quantify myelinated axon number, density, and myelin width as previously described [15,16]. All analysis was done by an observer blinded to the experimental groups.

2.2.6. *Nerve conduction velocity (NCV)*

NCV from mice tails were measured in a lab-built instrument inside a grounded Faraday cage. Mice were anesthetized using a constant flow of isoflurane. The external body temperature was maintained at 37 °C with a chargeable warm heating pad (Kent Scientific Inc). The body temperature was continuously monitored with a thermal camera (Micro-Epsilon). Tail skin and stainless steel recording electrodes (~29 ga, World Precision Instruments) were sanitized with 70% isopropanol. The recording electrodes were inserted 1 cm distal to the base of the tail. The nerve compound action potential was measured using an extracellular amplifier (DAM80, World Precision Instruments). Stimulating electrodes were inserted approximately 30 mm distal to the recording electrodes. *V*oltage pulses (2–5 msec duration, 0.6–4 V) were delivered to the stimulating electrodes from a battery powered stimulus

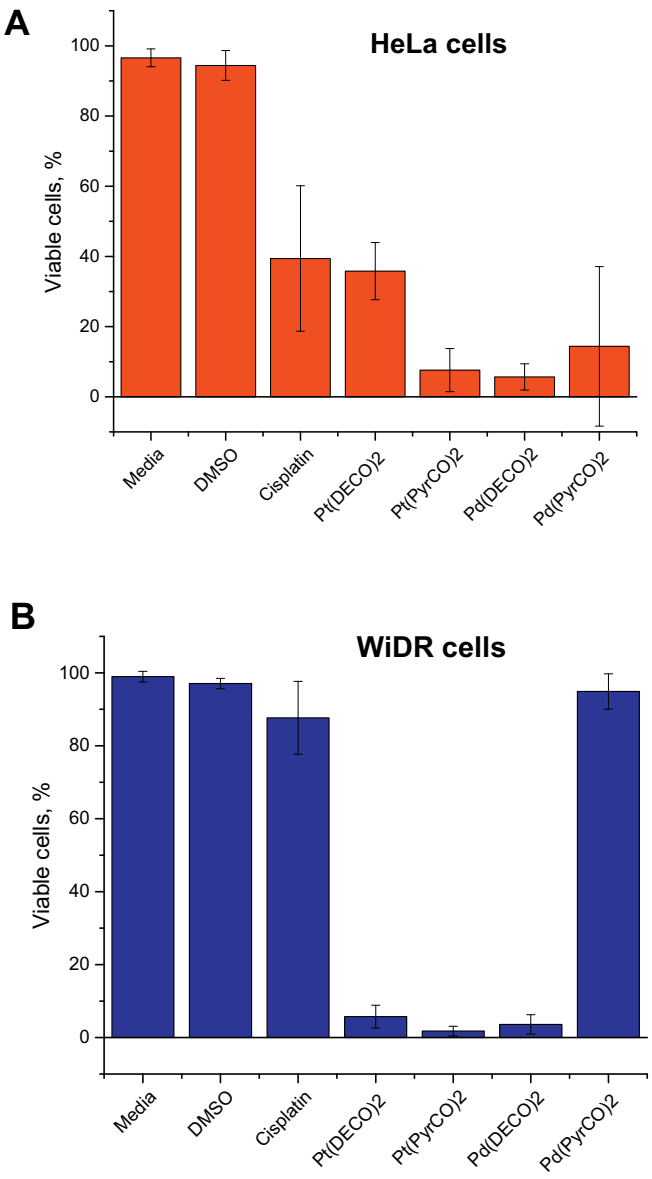

Fig. 5. Viability of the prepared complexes and A: HeLa cells and B: WiDr cells. After 24-h incubation

isolator (Model 2200, A-M Systems). Recorded data from the extracellular amplifier and from the stimulator were collected and analyzed with PowerLab 8/35 (ADInstruments Inc.) and used to calculate nerve conduction velocity of the compound action potential after completion of the experiment. Mice were returned to their home cages for recovery.

2.2.7. Blood analysis

The blood samples were used to analyze for cytokines, hemoglobin, white cells, and platelets. Blood was collected from the submandibular vein with a lancet. Mice were restrained by hand at the nape of the neck so there is minimum movement of the head and easy access to the mandibular vein. A one-time blood collection up to 100 μL was performed. The blood was kept in the EDTA-treated tubes on ice for less than an hour to avoid coagulation, and then transferred to Washington U. core facility for blood analysis. The whole blood samples were tested with Hemavet 1700 Veterinary Multispecies Hematology System (Drew Scientific Group Inc.). Blood smears were examined microscopically for red and white blood cell counts, hemoglobin, and platelet counts.

2.2.8. Cytokine analysis

EDTA-treated tubes of blood collected from mice at week 7 post-injections were placed on ice and then centrifuged (10,000 rpm, 4 °C, 10 min) to separate the red cells. The supernatant was placed at -80 °C. The cytokine levels in the supernatant were assessed using a commercially available, customized magnetic bead multiplex kit (Procartaplex Mouse Simplex beads for TNFa, IL-6, ThermoFisher). Cytokine analysis was performed using Mouse 10-Plex Panel for the Luminex™ Platform. The assays were performed according to the manufacturer recommended protocol, with the modification of performing an overnight +4 °C incubation for the multiplex cytokines. Milliplex Analyst 5.1.0.0 software was used to calculate the level of cytokine from the median fluorescence intensity (MFI) of each bead.

2.2.9. Cardiotoxicity

The hearts extracted from euthanized mice were fixed in 10% neutral buffered formalin. After fixation, the tissues were trimmed, processed according to standard procedures, paraffin-embedded, and sectioned at 5-μm thickness. The sections were stained with hematoxylin and eosin for histopathologic evaluation and imaged with a microscope (Olympus BX51) and a colour camera (Infinity 3.0).

3. Results and discussion of biological testing

3.1. Pt and Pd- cyanoximes show strong in vitro cytotoxicity

Both platinum complexes $Pt(DECO)_2$ and $Pt(PyrCO)_2$ were highly toxic to HeLA and WiDR cancer cells (Fig. 5A). $Pt(DECO)_2$ was equally toxic as cisplatin against HELA cells, but had much higher toxicity against WiDR cells than did cisplatin.. Low viability of the cells in the presence of $Pt(DECO)_2$ that destroyed 95% of WiDr cells and > 60% of the HeLa cells suggested high efficacy of the complex. The $Pt(PyrCO)_2$ showed even higher cytotoxicity destroying 96.4% of WiDr and 95.2% of HeLa cells.

Palladium complexes, especially $Pd(DECO)_2$, were also highly cytotoxic. After 24 h of treatment, 94% of HeLa and 98%% of WiDr cells were destroyed with $Pd(DECO)_2$ (Fig. 5). In comparison, the same concentration of cisplatin destroyed 55% of HeLa and only 12% of WiDR cells after 24 h. The $Pd(PyrCO)_2$ showed mixed results with somewhat lower efficacy against WiDR cells. The $Pd(PyrCO)_2$ complex, precipitates above the cell layer in the culture dish, which, apparently, explains its low cytotoxic activity.

PyrCO-based metal complexes showed lower water solubility. Both Pt (II) and Pd (II) complexes were relatively short-lived in aqueous buffers forming an insoluble layer above the cells by the end of 24 h incubation period. While being highly potent *in vitro*, low solubility of these complexes would lead to poor bioavailability of the complexes *in vivo*. For this reason, PyrCO complexes were excluded from *in vivo* testing. Pd(II) complexes only recently came into the spotlight as potential chemotherapy drugs [17,18]. Given that most approved metal based chemotherapy drugs are derived from Pt with its well documented side effects, we selected $Pt(DECO)_2$ for the *in vivo* toxicity evaluation.

3.2. $Pt(DECO)_2$ treated mice do not show sign of weight change

Loss of weight is one of the most common side effects of chemotherapy in humans and may occur as a result of stress, appetite loss, diarrhea, nausea and dehydration. The severe weight loss accompanied by rapid depletion of skeletal muscle mass during the chemotherapy treatment is clinically known as chemotherapy-induced cachexia [19]. This complex metabolic disorder frequently leads to a lethal outcome. Similar side effects are also observed in mice treated with many common chemotherapeutics. Thus, loss of weight > 10% has been observed in healthy mice treated with Folfox (a combination of oxaliplatin, 5-Fluorouracil, and leucovorin) [4]. Similar effects have been

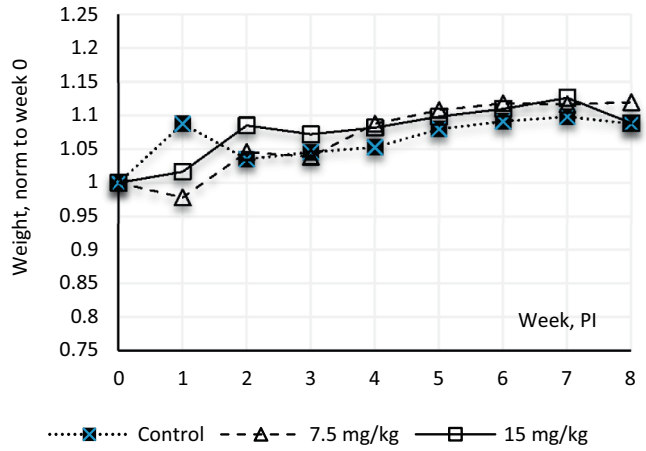

Fig. 6. Weight change of the mice treated with $Pt(DECO)_2$ All weights are normalized to the preinjection weight (week zero = 1). Control group was treated with a 5% dextrose solution.

found on oxaliplatin alone [20], cisplatin [21], and carboplatin treated mice [22]. In our study, mice treated with $Pt(DECO)_2$ did not show any change of the weight loss compared with the control, dextrose-treated group (Fig. 6). Gradual weight increase in the treated mice was similar to the typical increase of mass in healthy mice characteristic with the normal aging process.

3.3. $Pt(DECO)_2$ showed negligible myelotoxicity

Applications of chemotherapy drugs are frequently associated with a significant degree of myelotoxicity, leading to the decrease of the white blood cells. Common chemotherapy drugs can damage the red bone marrow, lowering the production of white cells, resulting in the decrease in the ability of the body to fight the microbial and fungal infection [2]. Lowered white blood cell counts accompanied with high fever, a condition known as febrile neutropenia, occurs in 25 to 40% of chemotherapy treated patients and reduces patient's quality of life and leads to hospitalization [23].

White blood cell counts reflect the ability of the animal to fight pathogens. Normal mouse white blood cell counts range from 2000 to 10,000/μL [24]. Our measurements showed that the $Pt(DECO)_2$ decreases the level of the white blood cells by an average of 35% from 8.8×10^3 per μl to 5.8×10^3 per μl after 7 weeks of treatments (Fig. 7a).

Previous studies have shown that a single dose of cisplatin at 12 mg/kg decreases the white blood cell count to ~ 50% relative to the controls [25]. In the case of $Pt(DECO)_2$, white blood cell counts only show a marginal decrease following a much higher accumulative dosage (7×15 mg/kg), making $Pt(DECO)_2$ significantly less myelotoxic than cisplatin. Importantly, even after 7 weeks of weekly high-dosage injections, the number of white blood cells (5500/μL) remain within the healthy limit (for mice: 2000–10,000/μL [24]).

In addition to the weakening of the immune system, chemotherapy induced myelotoxicity also leads to anemia in cancer patients due to the decrease of the red blood cells (RBCs) that carry oxygen from the lungs to the rest of the body. The decrease of RBCs is often worsened by the concomitant renal dysfunction that leads to the decline of erythropoietin, a hormone produced by the kidneys that stimulates RBC production [26]. Almost no changes in the RBC counts were observed after 7 weeks of treatment (Fig. 7b). The level of RBCs remained within the normal healthy range 7×10^6 to 13×10^6/μL [27]. In this study we also used hemoglobin as a marker of anemia. Hemoglobin values ranging from 13.6 to 16.4 g/dL are generally considered normal for adult male mice [28]. Mice treated with the high dose of $Pt(DECO)_2$ showed a small decrease in total hemoglobin to 12.5 g/dL (Fig. 7c).

The slightly decreased level of hemoglobin suggests a mild effect of $Pt(DECO)_2$ on the mice. A similar drop in hemoglobin in humans would not require any special treatment. Hemoglobin levels from 12.5 to 13.5 g/dL are considered very mild and from 10.7–12.4 g/dL are mild. The results from our study showed a very mild effect of the $Pt(DECO)_2$ on hemoglobin.

For many cancer treatments, chemotherapy is used to shrink the tumor. Then surgery is finally performed to remove the mass. If platelet counts are too low, surgery cannot be safely performed. The fact that $Pt(DECO)_2$ doesn't seem to impact platelet counts (Fig. 7d), with the normal range 3 to 10×10^5/μL [27], is a significant benefit.

3.4. Mice demonstrate no peripheral neurotoxicity

Chemotherapy-induced peripheral neuropathy (CIPN) is the most common neurological complication of cancer treatment [29]. This chronic painful condition causes severe debilitating symptoms leading to reduction of doses to mitigate CIPN or the premature terminations of treatment. The symptoms of CIPN (sharp and dull pain, loss of sensitivity, motor dysfunction) are varied and related to the specific toxicity

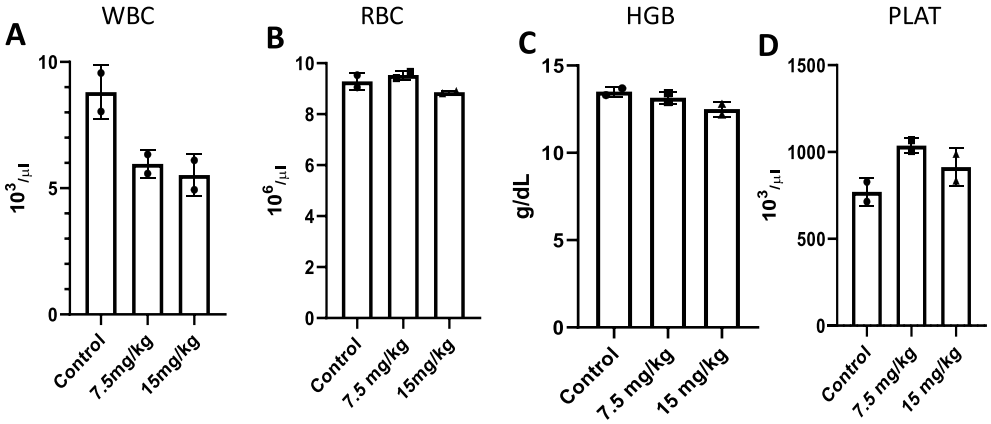

Fig. 7. Level of white blood cells (WBC), red blood cells (RGB), total hemoglobin (HGB), and platelets (PLAT) in the mice treated $Pt(DECO)_2$ at different dosages (ip, once/weekly). Control group mice were treatedwith a 5% dextrose solution (ip, once/weekly).The blood was collected from the mice after 7 weeks of weekly drug injections. (For interpretation of the references to colour in this figure legend, the reader is referred to the web version of this article.)

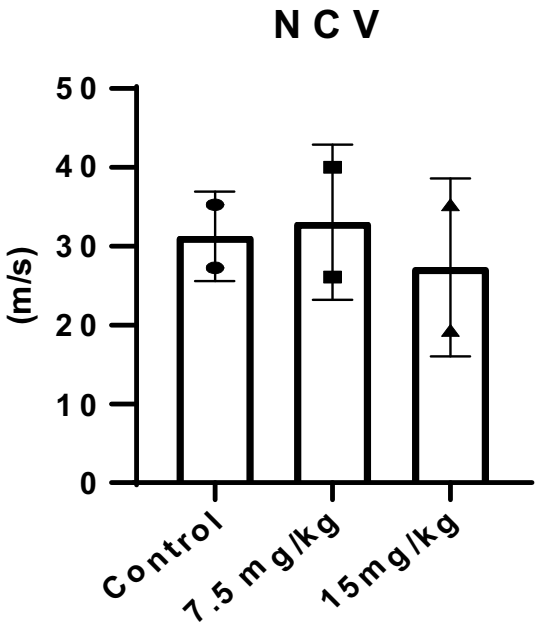

Fig. 8. Nerve conduction velocity measured caudally in mice treated with Pt(DECO)$_2$ for 8 weeks.

of the class of drugs involved. Nerve conduction velocity (NCV) is a frequent clinically used test for CIPN patients to evaluate both motor and sensory nerves [30]. NCV studies are considered the gold standard CIPN test in patients receiving platins family drugs [5]. A decrease in NCV is usually seen with many classes of chemotherapeutic drugs both in human and rodents. For example, cisplatin-treated animals usually confer a relatively small but significant reduction of the NCV when measured caudally ($-9\% \pm 3\%$, $p < 0.05$) [31]. Relatively low reduction in NCV even after a large dose of Pt(DECO)$_2$ (Fig. 8) suggests the stability of the myelinated fibers in the peripheral nerves.

To confirm the resistance of the fibers to the drug, we conducted nerve histomorphometry on sciatic nerves extracted from the mice after 8 weeks of treatment. Optical images of the nerves are shown in Fig. 9 and the derived quantitative parameters are shown in Table 1. No architectural changes were present in the nerves of the treated mice. Representative sections demonstrate normal myelinated fiber distribution with no evidence of myelinated fiber injury or myelinated fiber debris. The perineurium of the nerve fascicles shows normal architecture of perineural cells. Nerve endoneurium collagen and microvessels are normal in appearance absent of any edema or inflammatory cells.

Chemotherapy treatments are also linked to a variety of cognitive side effects that affecting thinking, learning, processing or remembering information. These side effects collectively known as “chemo brain” [32] are characterized by the release of pro-inflammatory cytokines that facilitate demyelination of neurons in the central nerve system. While hydrophilic chemotherapeutic agents usually cannot cross the blood-brain-barrier (BBB), cytokines such as tumor necrosis factor-alpha (TNF-α) and interleukin-6 (IL-6) can penetrate through the BBB and induce inflammatory responses in the brain.

While a low level of TNF-α protects the nerves [33], high level of this cytokine is often associated with demyelination of the neurons in the central nerve system. TNF-α elevation in plasma has long been implicated in demyelinating processes in the brain [34] and is considered as one of the main candidate mechanisms underlying cognitive

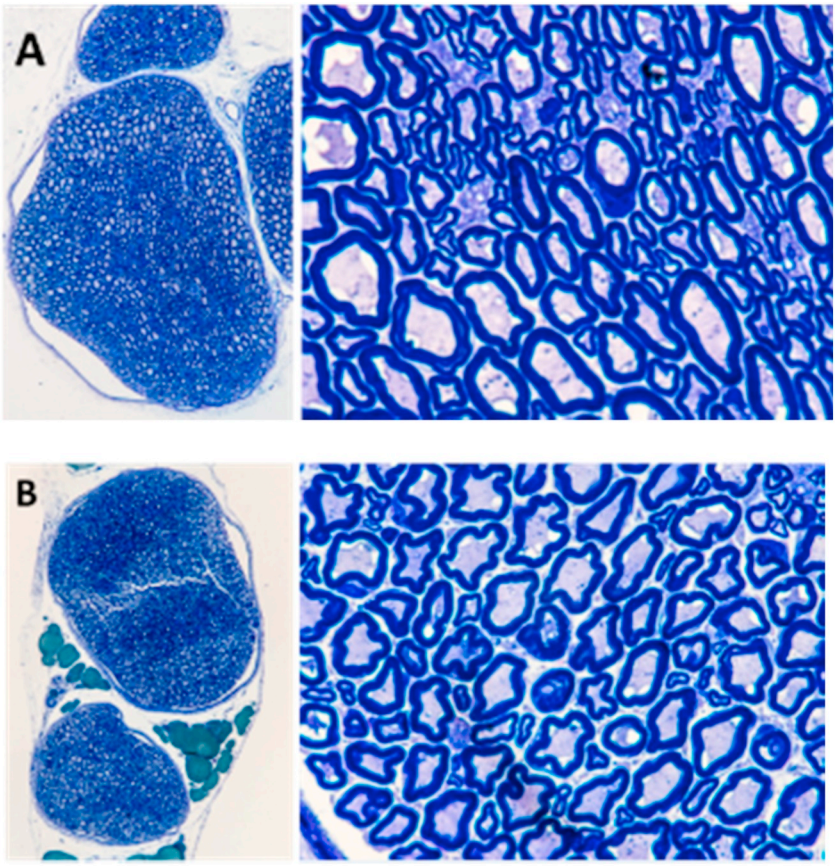

Fig. 9. Histology of the sciatic nerve. A: Control mice treated with a 5% dextrose solution; B: Mice treated with (Pt(DECO)$_2$, ip, 8 weeks, 15 mg/kg once/weekly). Sections were stained with OsO_4, and counterstained with toluidine blue. Each panel shows images with magnification 200× and 2000×. (For interpretation of the references to colour in this figure legend, the reader is referred to the web version of this article.)

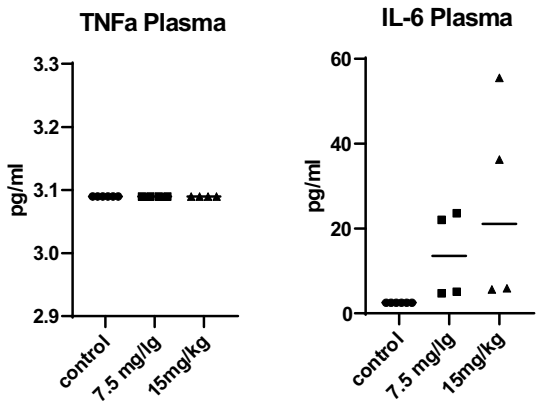

Fig. 10. Level of cytokines TNF-α and IL-6 in plasma following 8 weeks of weekly injections of Pt(DECO)2.

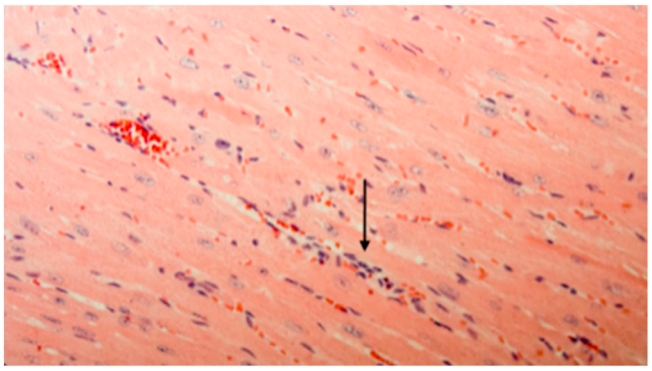

Fig. 11. Cardiac histology of mice treated with $Pt(DECO)_2$, 15 mg/kg, weekly, ip suggests low level of cardiotoxicity. A few minimal foci of increased interstitial cells in the myocardium can be seen (arrow). No necrosis of inflammation was noted. Magnification 400×.

impairment. Our study showed that the application of the $Pt(DECO)_2$ did not change the level of TNF-α in plasma (Fig. 10a), even at the maximum high dosage.

In contrast, the level of IL-6 turned out to be dose dependent reaching the relatively high level of > 50 pg/mL in one of the mice (Fig. 10b). IL-6 is a cytokine with complex pleiotropic functions, exerting positive and negative roles in homeostasis of many tissues. In a recent clinical study, the increased level of IL-6 has been correlated with a self-perceived cognitive disturbance in doxorubicin treated breast cancer patients [35]. Similar finding was observed in mice models [36] where the elevated level of circulating IL-6 has been shown to exert neurochemical modifications in the mice models of Alzheimer's disease, causing neuronal degeneration in the brain [36]. IL-6 is usually non-detectable in normal mice. However, it can reach a really high level as much as 10 ng/mL in certain animal models [37]. Nevertheless, the observed increase of circulating IL-6, introduces a potential risk factor and needs to be considered in greater details.

3.5. $Pt(DECO)_2$ shows negligible cardiotoxicity

Chemotherapy induced cardiotoxicity is one of the hallmarks of several anticancer drugs, such as doxorubicin [38]. Cardiotoxicity causes irreversible damage to the myocardium and leads to an important increase in morbidity and mortality in cancer patients. The knowledge of the onset of the cardiac dysfunction during chemotherapy and the susceptibility of patients to develop cardiotoxicity are scarce. Although several biomarkers have been proposed to predict the cardiotoxicity (*i.e.* serum troponin levels), the histology of the heart tissue considered to be the gold standard in preclinical studies. The histological evaluation of the heart excised from the control and treated mice showed no gross difference. There were no significant lesions noted in the heart across all groups. All samples from the mice, including controls showed a few minimal foci of increased interstitial cells in the myocardium of the left ventricle, with no associated necrosis or inflammation (Fig. 11).

3.6. $Pt(DECO)_2$ induces hepatotoxicity

Among the above-mentioned parameters, we also noted a sizable increase of the liver in the $Pt(DECO)_2$ treated animals *post mortem*. The effect was dose dependent with the greatest increase in mice treated with the highest dose. The hepatotoxicity occurs frequently in cancer patients treated with different chemotherapy drugs, including platinum complexes [39]. Acute and chronic damage to the liver can lead to a number of serious complications such as sinusoidal obstructive syndrome, steatosis, and pseudocirrhosis that are commonly associated with chemotherapies. These conditions can display clinical signs of acute hepatitis, liver cirrhosis, and even liver failure [40] and is one of the largest concerns in clinical oncology. Since the liver is the primary site of metabolism for many chemotherapy drugs, the interaction between the liver and $Pt(DECO)_2$ will have to be investigated in more details. The future study will also identify the mechanism of hepatotoxicity and whether the liver damage is reversible or can be prevented with adjuvant therapies.

4. Conclusions

Four new complexes of Pd and Pt with $DECO^-$ and $PyrCO^-$ cyanoxime anions were synthesized and characterized using spectroscopic methods and thermal analysis. Structures of several complexes were confirmed by the X-ray analysis. Platinum cyanoximates were found to be highly cytotoxic *in vitro* against two different types of human cancer cells, with several of the tested compounds out-performing cisplatin. Largely, $Pt(DECO)_2$ showed minimal *in vivo* toxicity. No changes were observed in the animal weight in the treated mice compared to the control dextrose-treated group. The levels of erythrocytes, leukocytes, hemoglobin, and platelets were within the normal level suggesting low myelotoxicity. NCV and nerve histomorphometry suggested no impact of $Pt(DECO)_2$ on the peripheral nerve architecture. Negligible cardiotoxicity was observed from the histological evaluation of the hearts from the treated animals. The complex, however, induced certain hepatotoxicity and lead to the elevation of IL-6, a pro-inflammatory cytokine. Overall, cyanoximates present promising candidate for future testing in the animal models of cancer.

Table 1
Quantitative parameters from representative sections from sciatic nerves of control and treated mice.

	Density fiber, per 100 μm^2	Fiber area, μm^2	Axon area, μm^2	Myelin area, μm^2	Fiber width, μm	G-ratio (Eq. diameter)
Control	261.17	32.14	12.43	20.39	4.92	0.58
$Pt(DECO)_2$ 15 mg/kg	266.54	26.38	10.21	16.79	4.75	0.61

Glossary and abbreviations

H(DECO)	2-oximino-2-cyano-N,N′-diethylacetamide
H(PyrCO)	2-oximino-2-cyan-N-pyrrolidineacetamide
ip	intraperitoneal injection
RGB	red blood cells
WBC	white blood cells
NCV	nerve conduction velocity
BBB	blood-brain-barrier

Declaration of competing interest

There is no conflict of interest between co-authors of this paper.

Acknowledgment

We are grateful to Prof. Viktor Nemykin (University of Manitoba) for preliminary structure determination of the red $[Pt(PyrCO)_2]_2$ dimer and Ms. Victoria Barry for invaluable technical help. We also thank Dr. Diana Bender from Bursky Center for Human Immunology & Immunotherapy Programs at Washington University for cytokine analysis and Ms. Suellen Greco from Washington University DCM Research Animal Diagnostic Laboratory for the histology of the heart. We also thank the Petroleum Research Fund for the award (NG) and the National Cancer Institute (R01 CA208623, MB) for funding.

Appendix A. Supplementary data

Supplementary data to this article can be found online at https://doi.org/10.1016/j.jinorgbio.2020.111082.

References

[1] S.M. Cohen, S.J. Lippard, Cisplatin: From DNA damage to cancer chemotherapy, Progress in Nucleic Acid Research and Molecular Biology, Academic Press, 2001, pp. 93–130.
[2] J.P. Curtin, W.J. Hoskins, S.C. Rubin, W.B. Jones, T.B. Hakes, M.M. Markman, B. Reichman, L. Almadrones, J.L. Lewis Jr., Chemotherapy-induced neutropenia and fever in patients receiving cisplatin-based chemotherapy for ovarian malignancy, Gynecol. Oncol. 40 (1991) 17–20.
[3] F. Cobo, G. De Celis, A. Pereira, X. Latorre, J. Pujadas, S. Albiol, Oxaliplatin-induced immune hemolytic anemia: a case report and review of the literature, Anti-Cancer Drugs 18 (2007) 973–976.
[4] R. Barreto, D.L. Waning, H. Gao, Y. Liu, T.A. Zimmers, A. Bonetto, Chemotherapy-related cachexia is associated with mitochondrial depletion and the activation of ERK1/2 and p38 MAPKs, Oncotarget 7 (2016) 43442–43460.
[5] V. Brozou, A. Vadalouca, P. Zis, Pain in platin-induced neuropathies: a systematic review and meta-analysis, Pain Ther 7 (2018) 105–119.
[6] A. Rossi, M.D. Maio, P. Chiodini, R.M. Rudd, H. Okamoto, D.V. Skarlos, M. Früh, W. Qian, T. Tamura, E. Samantas, T. Shibata, F. Perrone, C. Gallo, C. Gridelli, O. Martelli, S.-M. Lee, Carboplatin- or cisplatin-based chemotherapy in first-line treatment of small-cell lung cancer: the COCIS meta-analysis of individual patient data, J. Clin. Oncol. 30 (2012) 1692–1698.
[7] N. Gerasimchuk, C.L. Barnes, D. Boaz, Preparation, spectroscopic, and structural characterization of the first Co (III) cyanoxime complex: two polymorphs of fac-, tris (benzoylcyanoximato) cobalt (III), Co (BCO) 3, J. Coord. Chem. 63 (2010) 943–953.
[8] J. Ratcliff, P. Durham, M. Keck, A. Mokhir, N. Gerasimchuk, Part 2: in vitro cytotoxicity studies of two ML2 complexes (M = Pd, Pt; L = 2-cyano-2-isonitroso-N-morpholylacetamide, HMCO), Inorg. Chim. Acta 385 (2012) 11–20.
[9] D. Eddings, C. Barnes, N. Gerasimchuk, P. Durham, K. Domasevich, First bivalent palladium and platinum cyanoximates: synthesis, characterization, and biological activity, Inorg. Chem. 43 (2004) 3894–3909.
[10] N.G. Nikolay, G. Ilia, S. Pal, Structural peculiarities of cyanoximes and their anions: co-crystallization of two diastereomers and formation of acid-salts, Current Inorganic Chemistry (Discontinued) 5 (2015) 38–63.
[11] N. Gerasimchuk, M. Berezin, Near-Infrared Emitters, (2018) (Google Patents).
[12] D.R. Klaus, M. Keene, S. Silchenko, M. Berezin, N. Gerasimchuk, 1D polymeric platinum cyanoximate: a strategy toward luminescence in the near-infrared region beyond 1000 nm, Inorg. Chem. 54 (2015) 1890–1900.
[13] M. Hilton, N. Gerasimchuk, S. Silchenko, H.A. Charlier, Synthesis, properties and crystal structure of the 2, 4-dichlorophenyl-cyanoxime: a powerful carbonyl reductase inhibitor, J. Chem. Crystallogr. 43 (2013) 157–164.
[14] C. Cheadle, J. Ratcliff, M. Berezin, V. Pal'shin, V.N. Nemykin, N.N. Gerasimchuk, Shortwave infrared luminescent Pt-nanowires: a mechanistic study of emission in solution and in the solid state, Dalton Trans. 46 (2017) 13562–13581.
[15] D.A. Hunter, A. Moradzadeh, E.L. Whitlock, M.J. Brenner, T.M. Myckatyn, C.H. Wei, T.H. Tung, S.E. Mackinnon, Binary imaging analysis for comprehensive quantitative histomorphometry of peripheral nerve, J. Neurosci. Methods 166 (2007) 116–124.
[16] H. Zhou, Y. Yan, X. Ee, D.A. Hunter, W.J. Akers, M.D. Wood, M.Y. Berezin, Imaging of radicals following injury or acute stress in peripheral nerves with activatable fluorescent probes, Free Radic. Biol. Med. 101 (2016) 85–92.
[17] M. Tanaka, H. Kataoka, S. Yano, H. Ohi, K. Kawamoto, T. Shibahara, T. Mizoshita, Y. Mori, S. Tanida, T. Kamiya, T. Joh, Anti-cancer effects of newly developed chemotherapeutic agent, glycoconjugated palladium (II) complex, against cisplatin-resistant gastric cancer cells, BMC Cancer 13 (2013) 237.
[18] A.C. Caires, Recent advances involving palladium (II) complexes for the cancer therapy, Anti-Cancer Agents in Medicinal Chemistry (Formerly Current Medicinal Chemistry-Anti-Cancer Agents) 7 (2007) 484–491.
[19] L.E. Daly, E.B. Ni Bhuachalla, D.G. Power, S.J. Cushen, K. James, A.M. Ryan, Loss of skeletal muscle during systemic chemotherapy is prognostic of poor survival in patients with foregut cancer, J. Cachexia. Sarcopenia Muscle 9 (2018) 315–325.
[20] P. Marmiroli, B. Riva, E. Pozzi, E. Ballarini, D. Lim, A. Chiorazzi, C. Meregalli, C. Distasi, C.L. Renn, S. Semperboni, L. Morosi, F.A. Ruffinatti, M. Zucchetti, S.G. Dorsey, G. Cavaletti, A. Genazzani, V.A. Carozzi, Susceptibility of different mouse strains to oxaliplatin peripheral neurotoxicity: phenotypic and genotypic insights, PLoS One 12 (2017) e0186250.
[21] J.S. Damrauer, M.E. Stadler, S. Acharyya, A.S. Baldwin, M.E. Couch, D.C. Guttridge, Chemotherapy-induced muscle wasting: association with NF-κB and cancer cachexia, Eur J Transl Myol 28 (2018) 7590.
[22] B.A. Hain, H. Xu, J.R. Wilcox, D. Mutua, D.L. Waning, Chemotherapy-induced loss of bone and muscle mass in a mouse model of breast cancer bone metastases and cachexia, JCSM Rapid Commun 2 (2019).
[23] D.C. Dale, Colony-stimulating factors for the management of neutropenia in cancer patients, Drugs 62 (2002) 1–15.
[24] K.E. O'Connell, A.M. Mikkola, A.M. Stepanek, A. Vernet, C.D. Hall, C.C. Sun, E. Yildirim, J.F. Staropoli, J.T. Lee, D.E. Brown, Practical murine hematopathology: a comparative review and implications for research, Comp Med 65 (2015) 96–113.
[25] M.R. Nowrousian, C.G. Schmidt, Effects of cisplatin on different haemopoietic progenitor cells in mice, Br. J. Cancer 46 (1982) 397–402.
[26] P.A. Wood, W.J. Hrushesky, Cisplatin-associated anemia: an erythropoietin deficiency syndrome, J. Clin. Invest. 95 (1995) 1650–1659.
[27] M. McGarry, C. Protheroe, J. Lee, Cell differential assessments of peripheral blood films, Mouse Hematology: A Laboratory Manual, Cold Spring Harbor Laboratory Press, New York, 2010, pp. 39–42.
[28] B.M. Raabe, J.E. Artwohl, J.E. Purcell, J. Lovaglio, J.D. Fortman, Effects of weekly blood collection in C57BL/6 mice, J. Am. Assoc. Lab. Anim. Sci. 50 (2011) 680–685.
[29] G. Kannarkat, E.E. Lasher, D. Schiff, Neurologic complications of chemotherapy agents, Curr. Opin. Neurol. 20 (2007) 719–725.
[30] S. Sharma, R. Venkitaraman, P.R.J. Vas, G. Rayman, Assessment of chemotherapy-induced peripheral neuropathy using the LDIFLARE technique: a novel technique to detect neural small fiber dysfunction, Brain Behav 5 (2015) e00354.
[31] W. Boehmerle, P. Huehnchen, S. Peruzzaro, M. Balkaya, M. Endres, Electrophysiological, behavioral and histological characterization of paclitaxel, cisplatin, vincristine and bortezomib-induced neuropathy in C57Bl/6 mice, Sci. Rep. 4 (2014) 6370.
[32] X. Ren, D.K. St. Clair, D.A. Butterfield, Dysregulation of cytokine mediated chemotherapy induced cognitive impairment, Pharmacol. Res. 117 (2017) 267–273.
[33] E. Kemanetzoglou, E. Andreadou, CNS demyelination with TNF-α blockers, Curr Neurol Neurosci Rep 17 (2017) 36.
[34] X. Ren, J.T.R. Keeney, S. Miriyala, T. Noel, D.K. Powell, L. Chaiswing, S. Bondada, D.K. St. Clair, D.A. Butterfield, The triangle of death of neurons: oxidative damage, mitochondrial dysfunction, and loss of choline-containing biomolecules in brains of mice treated with doxorubicin. Advanced insights into mechanisms of chemotherapy induced cognitive impairment ("chemobrain") involving TNF-α, Free Radic. Biol. Med. 134 (2019) 1–8.
[35] Y.T. Cheung, T. Ng, M. Shwe, H.K. Ho, K.M. Foo, M.T. Cham, J.A. Lee, G. Fan, Y.P. Tan, W.S. Yong, P. Madhukumar, S.K. Loo, S.F. Ang, M. Wong, W.Y. Chay, W.S. Ooi, R.A. Dent, Y.S. Yap, R. Ng, A. Chan, Association of proinflammatory cytokines and chemotherapy-associated cognitive impairment in breast cancer patients: a multi-centered, prospective, cohort study, Ann. Oncol. 26 (2015) 1446–1451.
[36] M. Hüll, S. Strauss, M. Berger, B. Volk, J. Bauer, The participation of interleukin-6, a stress-inducible cytokine, in the pathogenesis of Alzheimer's disease, Behav. Brain Res. 78 (1996) 37–41.
[37] Y. Ma, M. Gao, H. Sun, D. Liu, Interleukin-6 gene transfer reverses body weight gain and fatty liver in obese mice, Biochim. Biophys. Acta (BBA) - Mol. Basis Dis. 1852 (2015) 1001–1011.
[38] D. Cardinale, M.T. Sandri, Role of biomarkers in chemotherapy-induced cardiotoxicity, Prog. Cardiovasc. Dis. 53 (2010) 121–129.
[39] A. Grigorian, C.B. O'Brien, Hepatotoxicity secondary to chemotherapy, J Clin Transl Hepatol 2 (2014) 95–102.
[40] A. Sharma, R. Houshyar, P. Bhosale, J.-I. Choi, R. Gulati, C. Lall, Chemotherapy induced liver abnormalities: an imaging perspective, Clin Mol Hepatol 20 (2014) 317–326.